DAMAGE TOLERANCE OF ENGINEERED CEMENTITIOUS COMPOSITES

VICTOR C. LI
Advanced Civil Engineering Materials Research Laboratory
Department of Civil and Environmental Engineering
University of Michigan, Ann Arbor, MI 48109-2125 USA

ABSTRACT

The experimental observations and measurements of damage tolerance of a fiber reinforced cement based matrix composite is reviewed in light of numerical analysis of damage development in a notched specimen. The extent of damage tolerance is found to depend both on details of the pre-peak uniaxial tensile stress-strain relationship as well as the post-peak stress-crack opening relationship. A synergistic effect is determined between on-fracture-plane energy absorption and off-fracture-plane energy absorption. Concepts for material engineering for damage tolerance of fiber reinforced brittle matrix composite are discussed.

KEYWORDS

Damage tolerance, brittle matrix composites, fiber reinforcement.

INTRODUCTION

This paper reviews the current knowledge of the damage tolerant behavior of Engineered Cementitious Composites (ECC) based on experimental observations and analytic modeling. ECC exhibits high tensile ductility reaching 5-8% and fracture toughness upwards of 30 kJ/m^2 approaching that of metals. ECC is a cement based matrix composite reinforced with a few volume % (usually less than 2%) of short randomly oriented fibers. The composite has been microstructurally engineered to strain-harden via multiple cracking in unaxial tension. Crack bridging model (Li, 1992) and steady state cracking concepts (Marshall and Cox, 1988) have been utilized in determining the conditions of strain-hardening (Li, 1993). The first studies of damage tolerance of ECC was reported in Li and Hashida (1993), and Maalej et al. (1995). Other mechanical properties of this material have been investigated (Li and Wu, 1992; Maalej and Li, 1994; Li et al, 1994). Constitutive modeling of ECC and numerical studies of its fracture behavior was conducted by Kabele and Horii (1996).

High damage tolerance is critical in safe operation of structures made of brittle materials in which crack growth and fracture failure may occur, especially near stress concentrators. Common locations are at cut-outs and near joints or anchorage zones. In the latter, interaction of the brittle material and other material such as steel often creates high stress regions in the brittle material. Damage tolerant behavior by redistribution of stress associated with inelastic deformation can be critical in preventing catastrophic structural failure.

Apart from summarizing our current state of knowledge of damage tolerance in ECC, a purpose of this paper is to demonstrate clearly that damage tolerance can be achieved in brittle matrix composites with discontinuous fibers, and that micromechanics tools can be applied to serve as systematic guidance in fiber, matrix and interface tailoring. In the following, some basic experimental observations of ECC are reviewed. Directions on materials tailoring to achieving damage tolerance in brittle matrix composites based on insights gained from analytic modeling of the fracture behavior of ECC are then presented.

BASIC EXPERIMENTAL OBSERVATIONS

Experimental observations discussed below refers to a ECC material with typical composition shown in Table 1. Details of specimen preparation and testing procedures can be found in the original publications by Li and co-workers referenced above. Specimen dimensions are summarized in Fig. 1 and Table 2.

Table 1: Matrix Mix Proportions (by weight)

Materials	Cement	Silica Fume	Superplasticiser	Water
Mix Proportions	1.0	0.10	0.01	0.27

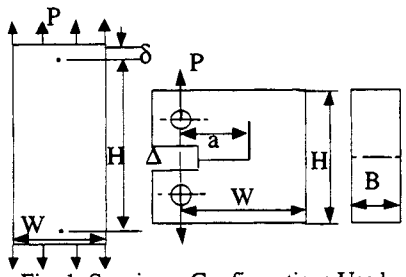

Fig. 1: Specimen Configurations Used

Table 2: Geometry of Fracture and UT Specimens

Specimen	W (mm)	H (mm)	B (mm)
Medium DCB	310	300	35
Large DCB	490	585	35
UT	76	207	13

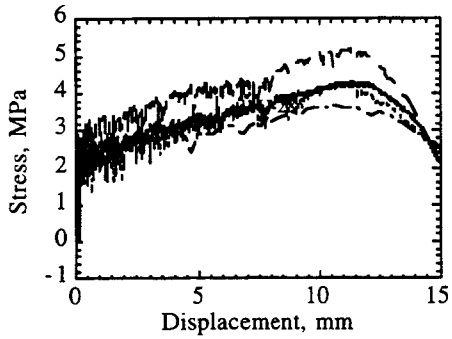

Fig. 2: Uniaxial Tensile Stress-Deformation Records for Un-notched Specimens

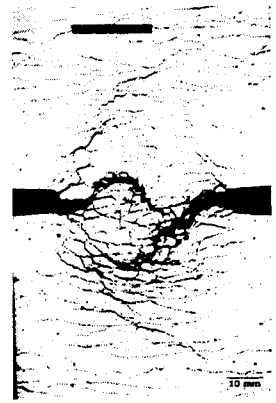

Fig. 3: Damage Pattern Of A Double-Edged-Notched Specimen of an ECC. Top marker shown is 20 mm

Uniaxial tensile behavior: ECC exhibits macroscopic strain-hardening (Fig. 2) after first cracking. With gage length of 207 mm, strain at peak load is approximately 5% in these specimens, compared with 0.01% tensile strain capacity in ordinary brittle cementitious materials. During strain-hardening, multiple cracks develop with continuously reducing crack spacing until localization occurs at one of these cracks. Because the multiple cracks evolve with rising applied load, the multiple cracks must be experiencing the rising branch of the bridging stress-crack width (σ–δ) relationship (Li and Leung, 1992). Subsequently the load drops

progressively with increasing crack opening associated with fiber pull-out at the localized fracture site. The fracture site is not necessary the first crack site, and multiple crack development appears randomly generated along the specimen length. The evolution of multiple cracks appears to be a stochastic process associated with distributed initial flaw sizes (Wu and Li, 1995). The final fracture site is likely a reflection of weaker maximum bridging strength either due to non-uniform fiber distribution, orientation or dispersion. While the sequence of multiple crack appearance follows the spatial distribution of matrix flaw size, final localization site is associated with the spatial distribution of maximum bridging strength of fibers along the specimen length.

Notch sensitivity: The effect of notches on the tensile strength of ECC was investigated with the same specimen as for the uniaxial tension test discussed earlier, but with variable double edge notch lengths. The damage pattern on a typical specimen tested to failure is shown in Fig. 3. It is seen that while cracking initiates in the region near the notch tips, the damage first spreads to other parts of the specimen with increasing load to distances many times the notch length, prior to localization into a tortuous fracture path connecting the notch tips.

A number of load-displacement curves are shown in Fig. 4. U-3 and U-7 have notch lengths of 15 mm, while U-4 and U-8 have notch lengths of 20 mm. The un-notched specimen U-28 is also included for comparison purposes. While the strain to failure seems to be reduced on the average, the notched specimens show the same as or even slightly higher tensile strength than the un-notched specimens. A usual means to demonstrate the notch-insentivity of materials is to plot the maximum load carried by the specimens as a function of reduced net section area. If the load capacity reduces linearly with the total notch length, then the material is notch insensitive. Notch-sensitive materials have load capacity reduction dropping at a faster rate than linear. Figure 5 shows the notch-sensitivity plot for the four notched specimens, and clearly indicates that at least for the notch depth used in this series of experiments, the ECC reveals notch-insensitive behavior under uniaxial tensile loading.

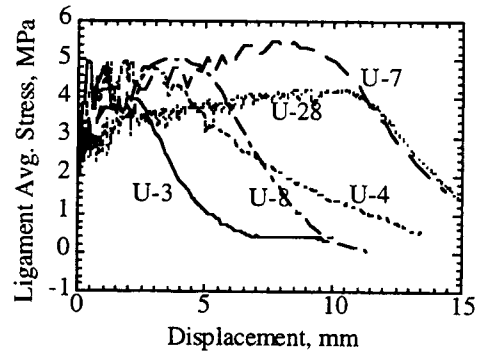

Fig. 4: Stress-Displacement curves for Notched specimens

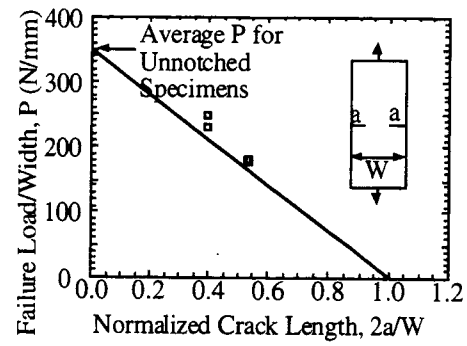

Fig. 5: Failure load vs notch depth relation

It is interesting to note the slightly higher tensile strength (Fig. 4) of ECC when notched compared to that of the unnotched specimens. It is possible that the presence of the notch confines the failure plane to be on the same plane as the notch, and therefore restricts the material from seeking out the plane with weakest bridging strength along the length of the specimen. The argument is analogous to the comparison between three point bend and four point bend test. In a three point bend test, there is only one (mid) plane which experience the highest stress and failure is therefore 'restricted' to that plane. In a four point bend test, there is a mid-span in which the bending stress is constant along the span, and therefore samples the weakest plane for failure. As a result, four-point bend tests usually reflect lower flexural strength than three point bend tests. This association of the final failure with the stocastic distribution of the weakest plane may explain the observed higher averaged tensile strength in the uniaxially loaded notched specimens.

Fracture behavior: The load-displacement curve of the large double cantilevered specimen of ECC is shown in Fig. 6. The damage development associated with the four stages indicated are shown in Figs. 7 a-d. At stage (a) shortly after the load-displacement curve turns non-linear, several matrix cracks can be observed on the specimen surface, emanating from or near the tip of the casted notch. For some specimens, the matrix cracks lie at very high angles and wing out at about 45° to the notch plane. At stage (b) close to peak load, the density of matrix cracks and the size of the damage zone has grown. Matrix cracks can be seen to initiate from the traction free notch surface, and the notch tip is visibly blunted by the matrix multiple cracking. At stage (c) just past peak load, the damage zone has grown further, with matrix cracks occuring at several notch length distances away and apparently not emanating from the notch tip. For the matrix cracks which did emanate from the notch tip, fracture localization is observed. The damage zone is shaped like a half-onion. At stage (d) well after peak load, further extension of the fracture zone and opening of the matrix cracks are observed. The more visible matrix crack band is inter-connected by another set of matrix cracks with smaller crack opening, often at right angles to the first set of matrix cracks. The tips of the half-onion are now located at the notch tip and at a point directly ahead of the notch at the specimen boundary.

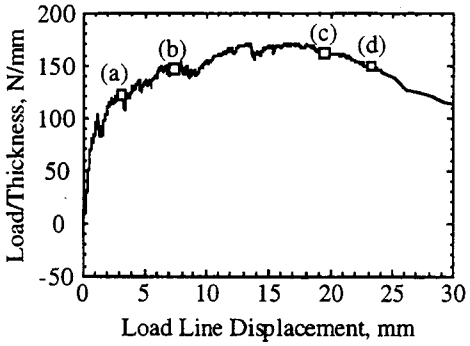

Fig. 6: Load-Displacement Curve Of A Double Cantilevered Beam (DCB) Specimen of ECC

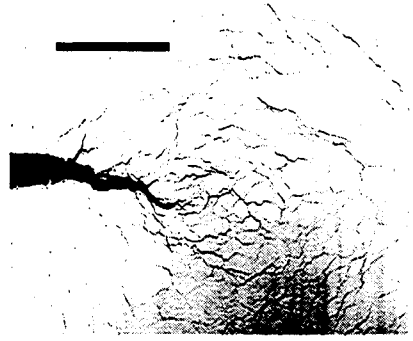

Fig. 8: Medium DCB Fracture Specimen Showing Damage Around Notch. Marker shown is 50 mm

In the specimen shown in Fig. 7, the damage zone appears non-symmetrical, with higher damage density to one side of the notch plane. The localized fracture zone, while connected to the notch tip, also appears to have nucleated at a small distance from the notch tip. This is probably associated with the stochastic nature of the matrix flaw spatial distributions. The blunted notch tip allows sampling and initiation of matrix cracks as well as determination of the final fracture plane not necessary confined to that of the casted-in notch. The damage zone of another specimen (medium DCB, Table 2), accentuating the half-onion shape and the two orthogonal sets of cracks, is shown in Fig. 8. The development of the damage zone responds to the load distribution in the specimen (Cox, 1991). The damage zone in the medium DCB may sense the presence of the specimen boundary and the compressive stress there more than the large DCB. The total fracture energy was measured and reported (Maalej et al, 1995) to be 27 kJ/m^2 and 34 kJ/m^2 for 2% and 3% fiber reinforcement. The maximum area of damage zone was observed to be 1150 cm^2 and 1220 cm^2 respectively.

J_R-curve: The J_R-curve provides a measure of fracture energy absorption as a function of crack extension. In a material like ECC where extensive damage occurs around the notch, the crack length cannot be measured. In fact, extension of the traction free crack is negligible even while J_R increases rapidly as the damage zone evolves. The best representation of this behavior is by plotting J_R against notch tip opening δ_t, shown in Fig. 9 (Li et al, 1995) for a ECC with V_f = 1%. The toughness (15 kJ/m^2) of the combined off-crack-plane damage process and the on-fracture-plane fiber pull-out process far exceeds the initial matrix toughness of 20 J/m^2.

For comparison purpose, the J_R-curves similarly measured for fiber reinforced cementitious composites and neat cement paste which do not show the damage tolerance observed in ECC are also included in Fig. 9. In addition to a higher value of steady value J_R, the ECC also shows a higher tangent modulus of the rate of increase of J_R with δ_t.

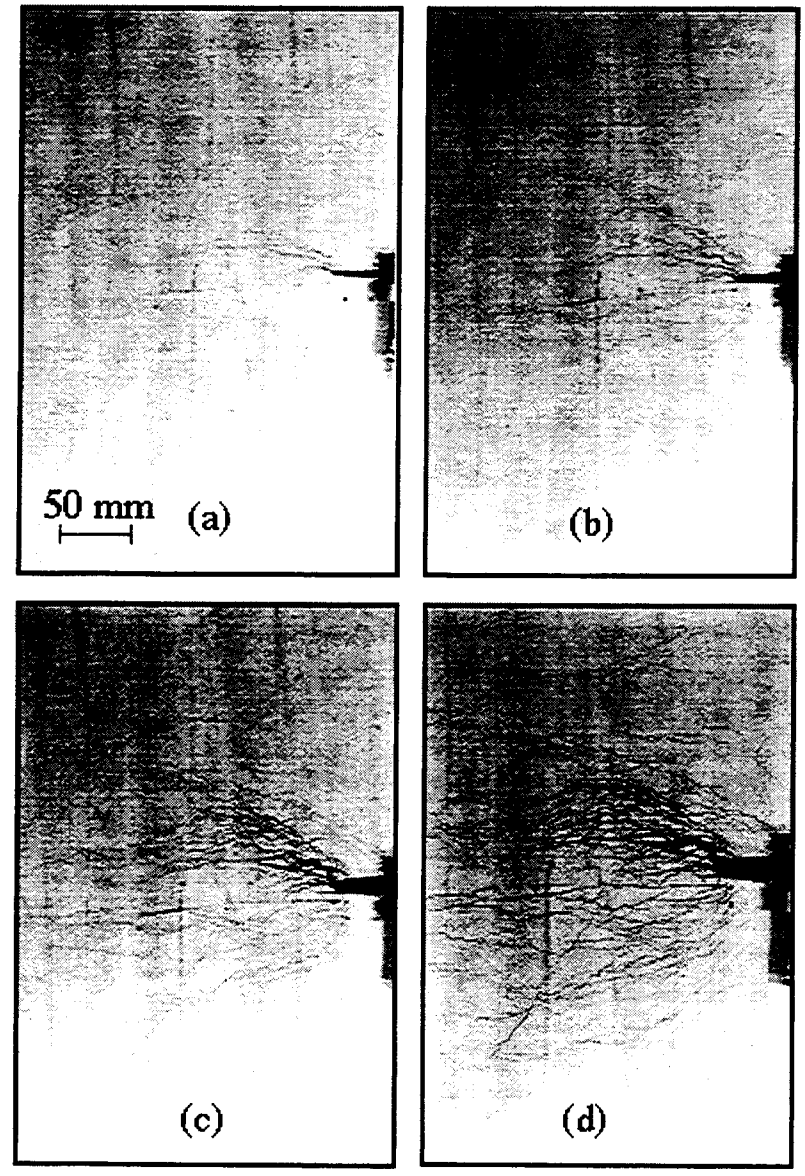

Fig. 7: DCB Damage Evolution as a Function of Deformation
(a) Δ = 3.10 mm (b) Δ = 7.32 mm (c) Δ = 19.45 mm (d) Δ = 23.16 mm

ANALYTIC MODELING AND MATERIALS ENGINEERING

While the ECC damage tolerant properties described above is exceptional in brittle matrix composites, these properties can be further improved with a better understanding of the controlling factors governing the development of the damage zone. In this section a constitutive model (Kabele and Horii, 1996) developed especially for the ECC described above, is used to draw insights on directions for materials engineering which may lead to enhancement of the damage tolerant behavior of ECC in particular, and of brittle matrix composites in general.

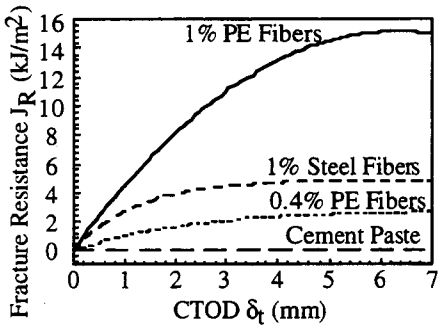

Fig. 9: J_R curve of ECC Compared with Ordinary FRC

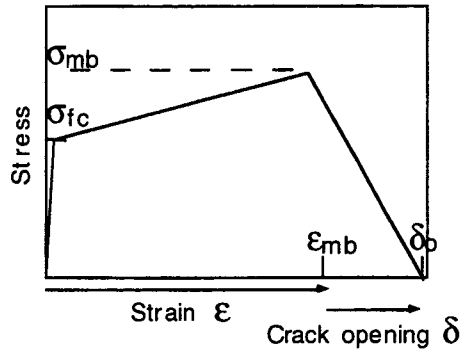

Fig. 10: Model Parameters

Constitutive model: The uniaxial response (Fig. 2) of ECC suggests two regimes of deformation behavior: Pre-peak stress-strain and post-peak stress-crack opening response. The pre-peak response has an inelastic strain-hardening behavior beyond first cracking strain. Furthermore since the strain-hardening behavior is associated with multiple cracking (cracking strain) of the brittle matrix, it is assumed that phenomenologically, 'yielding' is sensitive to the principal tensile stress only. The post-peak response is a localized fracture across which tension-softening and fiber pull-out occurs. The set of constitutive relations has the following important characteristics in relation to modeling ECC material response:

(1) The inelastic deformation due to multiple cracking is non-recoverable upon unloading.
(2) The Rankine yield function used ensures that inelastic response initiates whenever the principal tensile stress reaches the first crack strength. Further, the first set of multiple matrix cracks is initiated on planes normal to the maximum principal tensile stress.
(3) The kinematic hardening rule adopted implies that whenever strain-hardening occurs, the yield surface expands in stress space only in the direction of the cracking strain increment. This is physically appealing as the formation of a set of multiple cracks in one direction is not expected to influence the stress needed to generate a new set of multiple cracks in the orthogonal direction.
(4) The associated flow rule ensures that the source of inelastic strain derives from multiple cracking of the matrix, with strain increment due to crack opening parallel to the maximum principal tensile direction.

The above constitutive model of pre-peak and post-peak response of ECC in bi-axial stress state has been implemented in a coupled finite element - boundary element model. This numerical model has been verified by comparing model predictions with experimental observations for a variety of specimen geometry and loading configurations, including fracture, flexure and shear (Kabele and Horii, 1996; Kabele, 1995). In the following section, we deploy this model in the analyzes of ECC, with a view towards understanding the fundamental properties governing damage tolerance of this material.

To provide a sense of the capability of this model, we first summarize a simulation of damage evolution of the DCB using the Kabele-Horii model. The material parameters required for

prepeak response are E, ν, σ_{fc}, σ_{mb}, ε_{mb}, and for postpeak response are σ_{mb} and δ_0. E and ν are elastic modulus and Possions ratio. The first crack strength σ_{fc}, composite ultimate strength σ_{mb} and strain ε_{mb}, and the critical crack opening δ_0 are indicated on the uniaxial tensile stress-deformation curve illustrated schematically in Fig. 10. Details of the model parametric values employed and model results can be found in Kabele (1995).

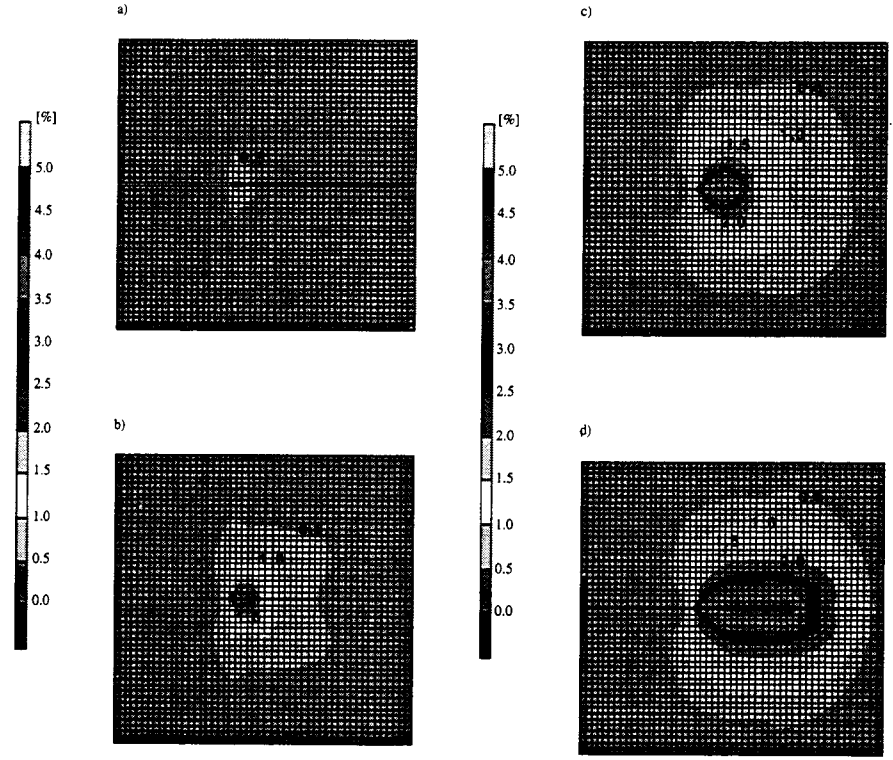

Fig. 11: Computed Evolution Of Damage Zone

Fig. 11 shows the evolution of the damage zone in the form of contour lines of maximum principal cracking strain for a medium size DCB. The four stages shown roughly correspond to those shown in Fig. 7. At stage A (Fig. 11a) just beyond the linear range, it is seen that a small damage zone has already developed. This damage zone evolves rapidly as peak load is approached (Fig. 11b). The onion shape damage zone (Fig. 11c) reveals itself clearly as stage C is reached, and the tip of the onion zone approaches the compression edge of the specimen ahead of the notch at stage D (Fig. 11d). Fig. 12 shows the direction and magnitude of the principal tensile strain near stage C. In the region near the notch (similar to that shown in Fig. 8), two orthogonal sets of cracking strains can be observed, with the magnitude of one set much larger than the other. The damage zone evolution and the dominant and minor sets of matrix cracks predicted are in strong resemblance to those observed and described in connection with Fig. 7.

In both Figs. 11 and 12, it can be observed that material points strained to cracking extends back behind the tip of the notch, implying matrix crack emanating from the notch surface. In addition, the extended zone of large inelastic deformation wrapped around the notch even before peak load (Fig. 11b) is indicative of blunting of the notch tip. Finally, the propagation of the traction free crack is predicted to be significantly delayed until much beyond the peak load (Fig. 11d). These model predictions are very consistent with experimental observations of ECC DCB specimens.

Materials engineering: Maalej et al (1995) found that the energy consumed in the formation of the damage zone can contribute to more than half the total fracture energy of the composite. This is also confirmed in numerical simulation by Kabele and Horii (1996). The off-fracture-plane energy consumption J_m can be used as a measure of damage tolerance of the ECC material.

Since the damage zone development is a direct result of the strain-hardening response of ECC, it is expected that the larger the difference between σ_{mb} and σ_{fc}, the larger is the damage zone and J_m. Similarly, since J_m results from inelastic strain energy consumption,the strain capacity ε_{mb} should also influence J_m. Finally, it may be expected that there is interplay between fracture energy consumed in the tension-softening process on the fracture plane and the off-fracture-plane damage development. The influence of prepeak stress-strain uniaxial tensile behavior and the synergistic effect of J_b on J_m are investigated using the Kabele and Horri model described above.

Numerical simulation of the large DCB specimen is conducted with variable σ_{mb} while all other parameters are fixed. J_m is computed by integration of the inelastic cracking strain in the damage zone at initiation of the traction free crack, normalized by the traction free crack extension. The J_m value at this loading stage is chosen because extension of the traction free crack is considered the beginning of steady state fracture extension. All computed results are summarized in Table 3. The universal case "univ" is used as the reference case when parametric values are varied.

Table 3: Numerical Calculation of Jm Dependence on Pre-peak and Post-peak Uniaxial Parameters Using the Kabele-Horii Model

Case ID	σ_{fc} (MPa)	σ_{mb} (MPa)	σ_{mb}/σ_{fc}	ε_{mb} (%)	δ_0 (MPa)	J_b (kJ/m^2)	J_m (kJ/m^2)
univ	2.20	4.32	1.96	5.78	0.66	14.3	27.9
smb-1	2.20	3.00	1.36	5.78	0.66	9.93	8.88
smb-2	2.20	3.36	1.53	5.78	0.66	11.1	12.6
sfc-1	1.00	4.32	4.32	5.78	0.66	14.3	34.6
sfc-2	1.50	4.32	2.88	5.78	0.66	14.3	33.3
e-1	2.20	4.32	1.96	2.00	0.66	14.3	11.2
e-2	2.20	4.32	1.96	4.00	0.66	14.3	18.5
d1	2.20	4.32	1.96	5.78	0.25	5.40	18.8
d2	2.20	4.32	1.96	5.78	0.45	9.72	21.4

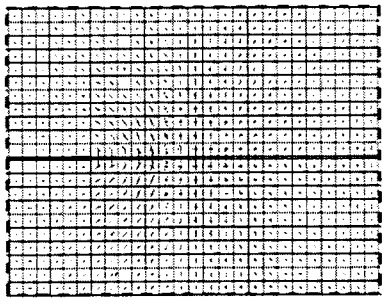

Fig. 12: Computed Principle Tensile Strain Field

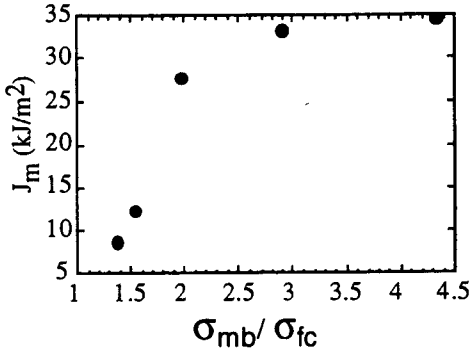

Fig. 13: Effect of σ_{mb}/σ_{fc} on J_m

i. Influence of prepeak stress-strain behavior on J_m: First, σ_{fc} is fixed at 2.2 MPa while σ_{mb} is varied (Case smb-1 and smb-2). As σ_{mb} approaches the first crack strength σ_{fc}, J_m rapidly drops towards zero. For σ_{mb} fixed at 4.32 MPa, J_m rapidly diminishes as σ_{fc} approaches the ultimate tensile strength σ_{mb} (Cases sfc-1 and sfc-2). These results can be combined into a plot of J_m against the ratio σ_{mb}/σ_{fc}, shown in Fig. 13. It is seen that J_m increases with this ratio as expected, but appears to saturate when this ratio exceeds about 2.5. It is not yet clear whether this saturation is real, or whether the damage zone extends to the boundary of the specimen and therefore saturates at higher values of σ_{mb}/σ_{fc}. Further computations are being conducted to confirm this point. The influence of ε_{mb} on J_m, with everything else fixed (e-1 and e-2) is shown in Fig. 14. The increasing trend of J_m with ε_{mb} is self-evident.

ii. Synergistic interactions between J_b and J_m: In the computation, J_b is varied by controlling δ_0 while keeping everything else fixed. The results, shown in Fig. 15 confirms a synergistic effect between J_b and J_m. The synergistic effect derives from an enlarged damage zone when the bridging zone on the main fracture plane is longer due to the larger value of δ_0.

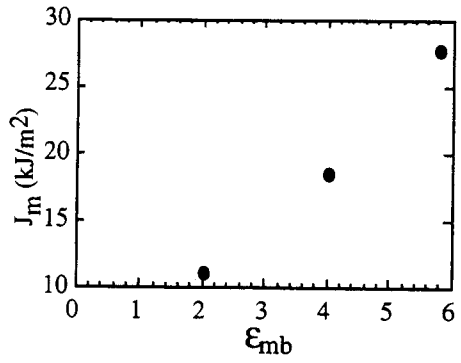

Fig. 14 Effect of ε_{mb} on J_m

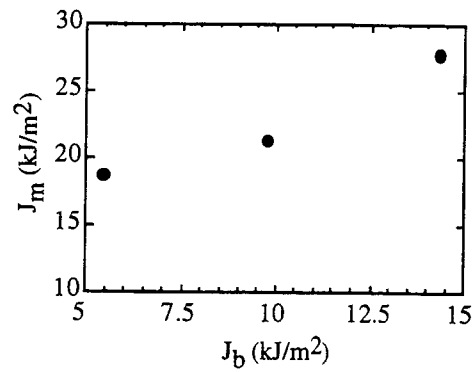

Fig. 15 Synergistic Effect of J_b on J_m

iii. Microstructure tailoring: Based on the results discussed above, it can be summarized that

$$J_m = \text{fcn}\left(\frac{\sigma_{mb}}{\sigma_{fc}}; \varepsilon_{mb}; J_b\right) \tag{1}$$

although σ_{mb}/σ_{fc} and ε_{mb} may not be independent of each other. The ratio σ_{mb}/σ_{fc} within certain limits can be designed. For example, the maximum bridging stress σ_{mb} is given by (Li, 1992)

$$\sigma_{mb} = \frac{1}{2} g \tau V_f \frac{L_f}{d_f} \tag{2}$$

where g is a snubbing factor (Li, 1992) related to inclined fiber bridging, τ is the fiber/matrix interface friction, V_f, L_f and d_f are the fiber volume fraction, length and diameter respectively. The maximum bridging stress σ_{mb} is governed mainly by fiber and interface parameters. Interface tailoring (Li and Stang, 1996) can be an effective means of achieving high damage tolerance.

The first crack strength σ_{fc} is mainly governed by matrix toughness and flaw size (Li and Leung, 1992). Matrix toughness can be controlled by aggregate content and water/cement ratio (Wittman, 1983), and potentially by addition of polymers. Flaw size can be controlled by processing means (mechanical force, particle size distribution control, chemical additives) to achieve desired packing density and flaw population.

Although both the prepeak stress strain curve and the post-peak tension-sofening curve are governed by fibers, it should be noted that J_b is controlled much more by the pull-out process of fibers, whereas the prepeak stress-strain curve is controlled mainly by the debonding process. Hybrid fiber system, for example, can be deployed to independently control the pre-peak stress-strain behavior and the post-peak tension-softening curve using two different fiber types.

FURTHER DISCUSSIONS AND CONCLUSIONS

From the experimental observations and analytic modeling described above, it is clear that ECC exhibits extensive damage tolerance as a brittle matrix composite. Even in the presence of a deep notch, ECC reveals strong capability of stress redistribution so that stress concentration detrimental to structural integrity is removed. The stress redistribution is accomplished by a combination of off-fracture-plane matrix cracking and inelastic energy dissipitation associated with fiber bridging (in the ascending branch of the $\sigma-\delta$ curve), and on-fracture-plane localized fracture with inelastic energy dissipation associated with fiber pull-out (in the descending branch of the $\sigma-\delta$ curve).

The analyses described also illustrates that macroscopically, the stress redistribution is achieved by the presence of a strongly non-linear tensile stress-strain relationship of ECC (Fig. 2). The non-linear behavior coupled with a large strain capacity ensures a ductile response in structural parts made from ECC, even in the presence of geometric discontinuities such as notches, cut-outs, connections or joints. Evans (1995) pointed out that materials with ductile non-linear response are "user-friendly" and innactly more reliable in structural design, as their strength are governed by Guassian rather than Weibull statistics. As a result, structural parts are not subject to size or scale effect, and the demand on material strength is lower. Design of structural parts with such materials follows that commonly used in metal structures.

Significant damage tolerance of ECC could not have been attained without the pseudo strain-hardening response under uniaxial tensile loading. Li (1993) found that to ensure pseudo strain-hardening, the fiber volume fraction V_f must be higher than a critical value given by

$$V_f^{crit} \equiv \frac{12 J_{tip}}{g\tau(L_f/d_f)\delta^*} \tag{3}$$

where J_{tip} is the crack tip toughness. δ^* is the crack opening at maximum bridging stress σ_{mb} in the $\sigma-\delta$ relation. For material engineering of damage tolerant composites, eqn. (3) provides a fundamental guideline for tailoring of fiber, matrix and interface properties. Beyond that, eqn. (1) allows further optimization of the pre-peak stress-strain and post-peak stress-deformation curve of the composite in controlling the extent of damage tolerance.

ACKNOWLEDGEMENTS

The research described in this paper has been supported by several NSF grants (MSS-9301949, BCS 9202097, CMS-9601262) to the ACE-MRL at the University of Michigan. Part of this work is a result of research collaborations between the ACE-MRL and the Applied Mechanics Laboratory directed by Prof. H. Horii at the University of Tokyo. Numerical computations leading to Figs. 11-15 have been carried out by Dr. P. Kabele at the University of Tokyo. His assistance in this work is greatly appreciated. In addition, the author would like to thank Dr. B. Cox, Dr. T. Hashida and Dr. M. Maalej for many helpful discussions in various aspects of damage tolerance of brittle matrix composites.

REFERENCES

Cox, B.N. (1991). Extrinsic factors in the mechanics of bridged cracks. *Acta Metall. Mater.* 39 1189-1201.

Evans, A.G. (1995). Design and life prediction issues for high-temperature engineering ceramics and composites: comparisons, contrasts and challenges. Harvard University Applied Mechanics Divison Report MECH 271.

Kabele, P. (1995). analytical modeling and fracture analysis of engineering cementitious composites. PhD Thesis, University of Tokyo.

Kabele, P. and H. Horii (1996). Analytical model for fracture behaviors of pseudo strain-hardening cementitious composites. *J. Materials, Conc. Struct., Pavements*, 532, 30, 209-219.

Li, V.C. (1992). Post-crack scaling relations for fiber reinforced cementitious composites, ASCE *J. of Materials in Civil Engineering*, 4, 1, 41-57.

Li, V.C. (1993). From Micromechanics to Structural Engineering – the Design of Cementitious Composites for Civil Engineering Applications. *JSCE J.* of *Struc. Mechanics and Earthquake Engineering*, 10, 2, 37-48.

Li, V.C. and T. Hashida (1993). Engineering ductile fracture in brittle matrix composites. *J. of Materials Science Letters*, 12, 898-901.

Li, V.C. and C.K.Y. Leung (1992). Steady state and multiple cracking of short random fiber composites, ASCE *J. of Engineering Mechanics*, 118, 11, 2246 - 2264.

Li, V.C., M. Maalej, and Y.M. Lim (1995). Fracture and flexural behavior in strain-hardening cementitious composites, in *Fracture of Brittle, Disorder Materials: Concrete, Rock and Ceramics* (G. Baker and B.L. Karihaloo, Eds.) pp. 101-114.

Li, V.C., D.K. Mishra, A.E. Naaman, J.K. Wight, J.M. LaFave, H.C. Wu and Y. Inada (1994). On the shear behavior of engineered cementitious composites, *J. of Advanced Cement Based Materials*, 1, 3, 142-149.

Li, V.C., and H. Stang (1996). Interface property characterization and strengthening mechanisms in fiber reinforced cement based composites. Submitted *to J. ACBM.*

Li, V.C., and H.C. Wu (1992). Conditions for Pseudo Strain-Hardening in Fiber Reinforced Brittle Matrix Composites. *J. Applied Mechanics Review*, 45, 8, 390-398.

Maalej, M., T. Hashida, and V.C. Li (1995). Effect of fiber volume fraction on the off-crack-plane fracture energy in strain-hardening engineered cementitious composites. *J. Amer. Ceramics Soc.*, 78, 12, 3369-3375.

Maalej, M. and V.C. Li (1994). Flexural/tensile strength ratio in engineered cementitious composites. ASCE *J. of Materials in Civil Engineering*, 6, 4, 513-528.

Marshall, D. and B.N. Cox. A J-Integral Method for Calculating Steady-State Matrix Cracking Stress in Composites," *Mechanics of Materials*, 7, pp 127 - 133, 1988.

Wittman, F. H. (1983). Structure of concrete with respect to crack formation, in *Frac. Mech. of Concrete* (Wittman, ed.) Elsevier, pp. 43-74.

Wu, H.C. and V.C. Li (1995). Stochastic process of multiple cracking in discontinuous random fiber reinforced brittle matrix composites. *Int'l J. of Damage Mechanics*, 4, 1, 83-102.